AGU PUBLICATIONS

Global Biogeochemical Cycles

RESEARCH ARTICLE
10.1002/2016GB005592

Key Points:
- Increasing global ocean winds over the last 27 years have significant regional impacts but little global effect on air-sea CO_2 fluxes
- Increases in CO_2 influx at high latitudes are fully offset by increases in efflux in the equatorial areas
- Efflux from the equatorial Pacific, caused by wind alone, has increased by 0.1 Pg C/yr over 27 years

Supporting Information:
- Supporting Information S1
- Figure S1
- Figure S2

Correspondence to:
R. Wanninkhof,
rik.wanninkhof@noaa.gov

Citation:
Wanninkhof, R., and J. Triñanes (2017), The impact of changing wind speeds on gas transfer and its effect on global air-sea CO_2 fluxes, *Global Biogeochem. Cycles*, *31*, 961–974, doi:10.1002/2016GB005592.

Received 28 NOV 2016
Accepted 7 MAY 2017
Accepted article online 9 MAY 2017
Published online 3 JUN 2017

The impact of changing wind speeds on gas transfer and its effect on global air-sea CO_2 fluxes

R. Wanninkhof[1] and J. Triñanes[1,2,3]

[1]Atlantic Oceanographic and Meteorological Laboratory, National Oceanic and Atmospheric Administration, Miami, Florida, USA, [2]Laboratory of Systems, Technological Research Institute, Universidad de Santiago de Compostela, Campus Universitario Sur, Santiago de Compostela, Spain, [3]Cooperative Institute for Marine and Atmospheric Studies, Rosenstiel School of Marine and Atmospheric Science, University of Miami, Miami, Florida, USA

Abstract An increase in global wind speeds over time is affecting the global uptake of CO_2 by the ocean. We determine the impact of changing winds on gas transfer and CO_2 uptake by using the recently updated, global high-resolution, cross-calibrated multiplatform wind product (CCMP-V2) and a fixed monthly pCO_2 climatology. In particular, we assess global changes in the context of regional wind speed changes that are attributed to large-scale climate reorganizations. The impact of wind on global CO_2 gas fluxes as determined by the bulk formula is dependent on several factors, including the functionality of the gas exchange-wind speed relationship and the regional and seasonal differences in the air-water partial pressure of CO_2 gradient (ΔpCO_2). The latter also controls the direction of the flux. Fluxes out of the ocean are influenced more by changes in the low-to-intermediate wind speed range, while ingassing is impacted more by changes in higher winds because of the regional correlations between wind and ΔpCO_2. Gas exchange-wind speed parameterizations with a quadratic and third-order polynomial dependency on wind, each of which meets global constraints, are compared. The changes in air-sea CO_2 fluxes resulting from wind speed trends are greatest in the equatorial Pacific and cause a 0.03–0.04 Pg C decade^{-1} increase in outgassing over the 27 year time span. This leads to a small overall decrease of 0.00 to 0.02 Pg C decade^{-1} in global net CO_2 uptake, contrary to expectations that increasing winds increase net CO_2 uptake.

Plain Language Summary The effects of changing winds are isolated from the total change in trends in global air-sea CO_2 fluxes over the last 27 years. The overall effect of increasing winds over time has a smaller impact than expected as the impact in regions of outgassing is greater than for the regions acting as a CO_2 sink.

1. Introduction

Significant progress has been made in quantifying different components of the bulk formulation of global air-sea carbon dioxide (CO_2) fluxes:

$$F = k\, s\, \Delta pCO_2 = \Gamma\, \Delta pCO_2 \tag{1}$$

where ΔpCO_2 is the air-water pCO_2 difference ($pCO_{2w} - pCO_{2a}$), referred to as the thermodynamic component; k is the gas transfer velocity, referred to as the kinetic component of the bulk flux expression; and s is the solubility of CO_2 in seawater. The product of k and s is referred to as the gas exchange coefficient, Γ [*Boutin and Etcheto*, 1997], or gas transfer coefficient [*Takahashi et al.*, 2009]. The parameter Γ is used to express the kinetic control of gas transfer.

The ΔpCO_2 is determined at ever greater fidelity through its automated acquisition on ships of opportunity and collation of data into unified data sets [*Takahashi et al.*, 2009, 2014; *Bakker et al.*, 2016]. Uncertainty in the parameterization of global gas transfer velocities has decreased through dedicated field process studies and syntheses. Local estimates based on purposeful tracer studies [*Ho et al.*, 2011] have shown excellent correspondence with global estimates based on ^{14}C inventories [*Peacock*, 2004; *Sweeney et al.*, 2007]. While many parameterizations of gas exchange with wind have been developed, the most frequently used are similar and contribute less than 15–20% to the uncertainty in k and the bulk CO_2 flux [*Ho et al.*, 2011; *Wanninkhof*, 2014].

Bulk formulations for air-sea mass and heat fluxes are commonly used to estimate global uptake, but they are a simplified expression for the complex transfer mechanism at the interface. Other means of determining CO_2 gas fluxes rather than the bulk formulation have been developed for estimates on local scales, notably the eddy correlation techniques [*Businger and Delaney*, 1990; *Butterworth and Miller*, 2016]. The bulk formulation expressed in equation (1) does not explicitly define the reference points for air and water measurements. Measurements of pCO_{2w} are commonly performed at ≈5 m depth from the ship's seawater intake and at ≈10 m height at the bow of the ship for pCO_{2a}. However, from a mechanistic perspective the reference heights should be the top and bottom of the liquid boundary layer of ≈100 μm thickness. Concentration gradients in aqueous CO_2 between the level of measurement and the near surface due to stratification and the net cool-skin effect can cause significant discrepancies in estimates of CO_2 uptake [*Van Scoy et al.*, 1995; *McNeil and Merlivat*, 1996].

In the following discussion, near-surface gradients in pCO_2, impacts of wind on surface water CO_2, and changes in ΔpCO_2 on air-sea CO_2 fluxes over time are not discussed. Rather, a single aspect of the impact of changing winds is investigated, namely, the effect of changes in wind speed on Γ and the resulting effect on air-sea CO_2 fluxes. The effect of the trends in wind on Γ in determining global CO_2 fluxes has received less attention than changes in surface water pCO_2 [*Le Quéré et al.*, 2010; *Sutton et al.*, 2014]. In modeling and observation-based extrapolations, the total effect of wind on k and ΔpCO_2 on air-sea CO_2 fluxes is usually reported [*Landschützer et al.*, 2014; *Rödenbeck et al.*, 2014].

The choice of wind product can have a significant effect on the overall uncertainty in global k [*Olsen et al.*, 2005]. Global wind products show appreciable differences in magnitude on regional and global scales [*Wallcraft et al.*, 2009], but most show increases over time that are modulated by large climate reorganizations such as the North Atlantic Oscillation, NAO, Southern Annular Mode, SAM, and El Niño/Southern Oscillation, ENSO [*Young et al.*, 2011; *Kent et al.*, 2013]. When comparing the differences in wind on Γ and on the resulting CO_2 fluxes, they generally scale with the magnitude of the global average wind speed. A bias in global wind speed of 1 m s^{-1} will cause a −0.2 Pg C bias in global CO_2 flux with higher winds causing greater uptake.

Trends in the magnitude of the wind and their impact on global air-sea CO_2 fluxes, both globally and in specific key regions, are investigated over the 27 year record. Three regions of particular importance in global air-sea CO_2 fluxes, and which show significant trends over time, are detailed. Using the delineations of *Takahashi et al.* [2009], these regions are the equatorial Pacific (14°N–14°S), polar Southern Ocean (50–62°S), and polar Atlantic Ocean (>50°N). A single wind speed product, cross-calibrated multiplatform (CCMP)-V2 [*Atlas et al.*, 2011], and a single monthly pCO_2 climatology with a reference year of 2005 [*Takahashi et al.*, 2014] are used. Two different functionalities of k with wind speed are investigated that meet the global ^{14}C constraints but differ in their wind speed dependence [*Wanninkhof et al.*, 2009].

2. Methods

For this effort, the cross-calibrated multiplatform (CCMP) wind product is used [*Atlas et al.*, 2011], which has been updated, reprocessed, and extended from July 1987 to May 2016. The analysis described below uses full calendar years and was performed prior to release of the 2015 and 2016 data in early October 2016. Therefore, it covers 27 years, from 1988 to 2014. The CCMP-V2 data were obtained from www.remss.com/measurements/ccmp and are described in detail on this site. In short, the CCMP-V2 is a level 3 ocean vector wind analysis product. The gridded 6-hourly, 0.25° surface vector winds are produced using a combination of satellite, moored buoy, and model wind data from the ECMWF Interim Reanalysis, ERA-Interim. The satellite observations include version 7 Remote Sensing Systems radiometer wind speeds, as well as QuikSCAT and ASCAT (advanced scatterometer) scatterometer wind vectors. The scalar winds in CCMP-V2 are similar to the ERA-Interim wind fields. The high resolution of the wind product facilitates capture of high-frequency events and, in particular, provides an accurate estimate of the variability in wind that is necessary to capture the second moment, $<u_{10}^2>$, and third moment, $<u_{10}^3>$, used in the parameterizations of gas exchange with wind.

For this analysis the 6-hourly, 0.25° $<u_{10}>$, $<u_{10}^2>$, and $<u_{10}^3>$ data were binned into monthly 1° by 1° pixels. *Kent et al.* [2013] compared several global products and showed that the CCMP winds were the most robust

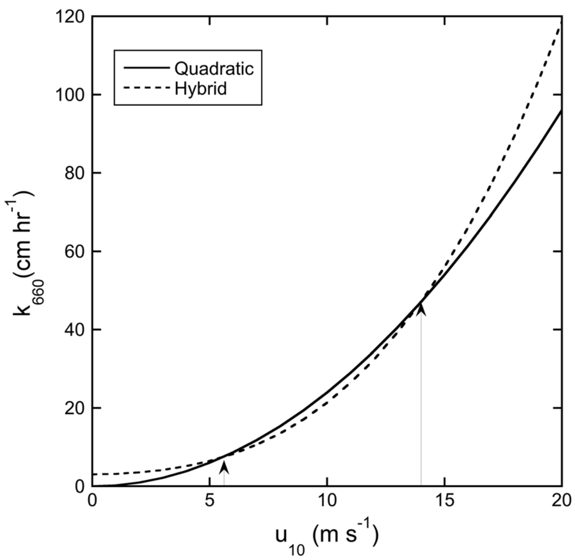

Figure 1. Relationship of gas exchange with wind speed. The solid line is the quadratic expression (equation (2)), and the dashed line represents the hybrid expression (equation (3)). Vertical arrows at 5.6 m s^{-1} and 14 m s^{-1} indicate where the relationships cross. For winds between 5.6 m s^{-1} and 14 m s^{-1}, the quadratic relationship yields larger gas transfer velocities than the hybrid expression.

in being bias free compared to in situ estimates. The CCMP product provides high-resolution coverage over the oceans and captures variability quite well. However, the representation of high wind events of short duration over a small area in long-term global records is challenging. This is largely addressed by using the second (and third) moments of the monthly averaged 6-hourly 0.25° winds in the parameterizations rather than using mean winds and relying on inferred wind speed distributions [*Monahan*, 2006].

An important caveat should be noted in our analysis. The CCMP product documentation cautions against interpreting trends in the product, as artificial trends can be introduced into a timeseries by changes in the observation array. As this is the very aspect we investigate, the trends and magnitudes of the wind in the CCMP product were spot checked with time series from select moorings in the Tropical Ocean–Global Atmosphere Tropical Atmosphere Ocean array and with National Data Buoy Center moorings 41002, 42036, and 42002 along the U.S. East Coast and Gulf of Mexico (www.ndbc.noaa.gov). These records showed similar trends and magnitudes as those observed in the CCMP product. Data from these platforms were incorporated into the CCMP product as well but weighted with other input streams such that they offered a quasi-independent verification that the trends were not artifacts. The observed large-scale trends in wind have also been observed in other wind products [*Kent et al.*, 2013].

To estimate the trends in air-sea CO_2 fluxes caused by changing winds and wind variability, two different parameterizations of gas transfer with wind were used. These parameterizations differ in their assumed functionality of gas transfer with wind as described in *Wanninkhof et al.* [2009]. Both are constrained on a global scale by the bomb ^{14}C inventory in the ocean [*Sweeney et al.*, 2007].The first assumes a quadratic dependency with wind

$$k_{660} = 0.24 \langle {u_{10}}^2 \rangle \tag{2}$$

while the second uses a polynomial expression, referred to as a hybrid expression:

$$k_{660} = 3 + 0.1 \langle u_{10} \rangle + 0.064 \langle {u_{10}}^2 \rangle + 0.011 \langle {u_{10}}^3 \rangle \tag{3}$$

where u_{10} (in m s^{-1}) are the wind speeds at 10 m height for neutral boundary conditions as provided by a monthly mean CCMP-V2 product binned on a 1° grid and k_{660} is the gas transfer velocity at a Schmidt number of 660 that, by convention, is expressed in cm h^{-1} (Figure 1). The Schmidt number is the kinematic viscosity of seawater divided by the diffusivity of the gas in question. The gas transfer velocity of CO_2 for a given Schmidt number is

$$k = k_{660}\left(Sc_{\mathrm{CO2}}/660\right)^{-1/2} \tag{4}$$

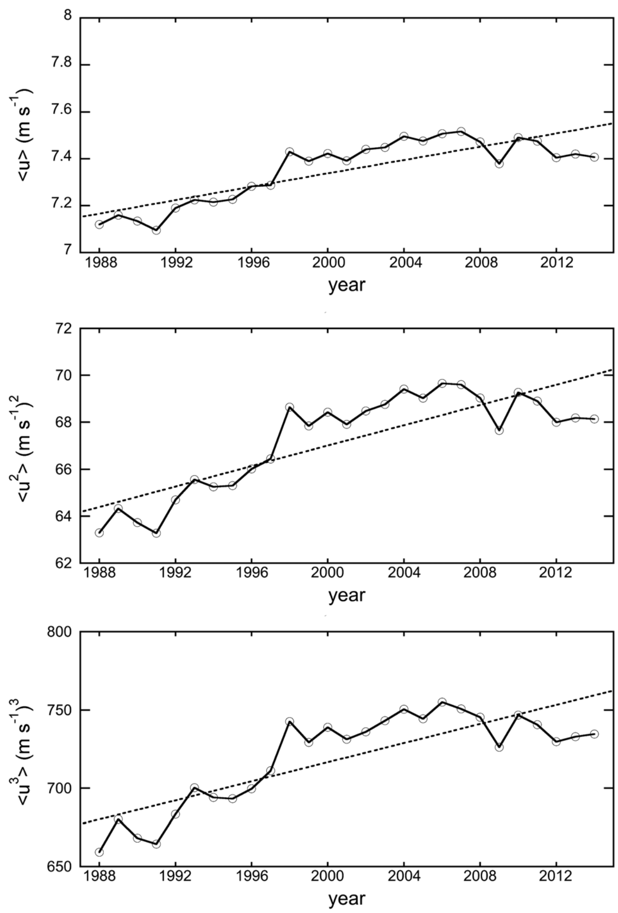

Figure 2. (top) Global trends in the annual wind speed, <*u*>, with a least squares linear fit and a slope of 0.14 m s^{-1} $decade^{-1}$ from 1988 to 2014, $r^2 = 0.71$. (middle) Second moment of the wind, $<u^2>$, with a slope of 2.1 $(m\ s^{-1})^2$ $decade^{-1}$, $r^2 = 0.69$. (bottom) Third moment of the wind, $<u^3>$, with a slope of 30.5 $(m\ s^{-1})^3$ $decade^{-1}$, $r^2 = 0.67$.

The dimensionless Schmidt number of CO_2 in seawater is expressed as a function of sea surface temperature (SST) according to *Wanninkhof* [2014]:

$$Sc_{CO2} = 2116.8 – 136.25\ SST + 4.7353\ SST^2 – 0.092307\ SST^3 + 0.0007555\ SST^4 \quad (5)$$

To determine the flux, the solubility of CO_2 in seawater, *s*, needs to be known, and the expression *s* as a function of salinity and temperature of *Weiss* [1974] is used. Both the Schmidt number and solubility of CO_2 are strong decreasing functions with temperature. However, the effect of temperature on *s* and $(Sc_{CO2}/660)^{-1/2}$ is opposite. Therefore, the product of *k* and *s* (Γ) has a weak dependence on temperature. This is shown in the supporting information where *s*, *Sc*, and $((Sc_{CO2}/660)^{-1/2}\ s)$ for CO_2 are plotted against temperature (Figure S1).

The direct impacts of wind speed on Γ and on air-sea CO_2 fluxes were investigated using an observation-based fixed monthly climatology of the air-water partial pressure of CO_2 difference, ΔpCO_2. An updated version of this monthly ΔpCO_2 climatology centered on the year 2005 was applied in this exercise [*Takahashi et al.*, 2014]. Data adjustments and temporal and spatial gap filling are as described in *Takahashi et al.* [2009]. Winds can have a direct influence on pCO_{2w} by causing upwelling of high CO_2 waters and entrainment of nutrients in surface water. The latter will increase biological productivity and lower the pCO_{2w}. The air-sea CO_2 fluxes themselves can also change the pCO_{2w} due to a loss or gain of CO_2 in the water. However, this effect is relatively small compared to other factors influencing pCO_{2w} due to the buffering capacity of the seawater carbonate system. The impacts of wind on pCO_{2w} are not incorporated into this analysis as the focus is on the kinetic component.

Few global wind speed records exist of sufficient duration and high enough resolution to accurately capture the trends in wind on Γ and air-sea CO_2 fluxes due to the limited instrumental record. For global coverage, satellite observations began in the mid-1980s, with records that span less than 30 years. While the CCMP-V2 data used here are processed in a consistent fashion, the number of input data varies over time and, as noted above, could impact the trend.

The effects of the combined changes in ΔpCO_2 fields and wind over time, and its effect on global CO_2 fluxes using different observation-based approaches, are shown in *Rödenbeck et al.* [2015]. A summary of numerical model outputs describing the temporal trends in air-sea CO_2 fluxes is provided in *Wanninkhof et al.* [2013]. The results of these works compared to this analysis show that changes in ΔpCO_2 have a controlling

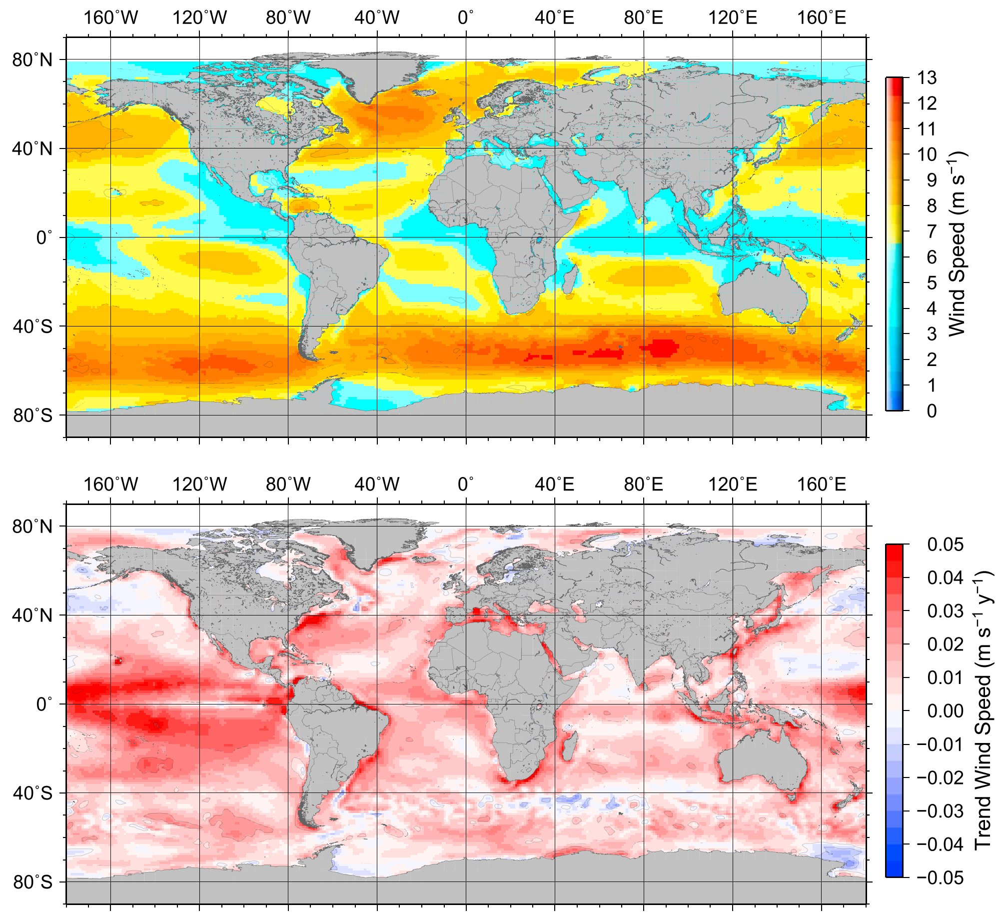

Figure 3. (top) Map of the annual average global wind speeds (m s^{-1}) for 2014. (bottom) Map of linear trend in wind speed from 1988 to 2014 (m s^{-1} y^{-1}).

influence on variability and trends in CO_2 fluxes. We isolated the impact of wind on Γ from the effects of Δ$p$$CO_2$ by using a fixed monthly averaged $p$$CO_2$ product. This aspect of the impact of changing winds and the wind variability of fluxes has not received much attention when studying changes in global air-sea CO_2 fluxes in a changing ocean.

Gas transfer velocities are assumed to be a function of the wind speed squared or a third-order polynomial (hybrid) such that the wind speed squared (second moment) and wind speed cubed (third moment) are important contributors to changes in k in addition to the mean wind speed. The global trends in $<u_{10}>$, $<u_{10}^2>$, and $<u_{10}^3>$ over the 27 year period are shown in Figure 2. To minimize the possibility of spurious results due to the seasonality of wind, the partial annual records from July–December 1987 and January–July 2015 were not included in the statistical analyses. The data were not deseasonalized or despiked prior to trend analyses. These procedures can make decadal trends statistically more robust but can also cause artifacts if residuals are not random. An inspection of the record showed that the decadal trends in wind in several regions were a composite of multiyear anomalies caused by the impacts of climate modes such as the NAO, SAM, or ENSO.

3. Results and Discussion

3.1. Global Long-Term Trends in the Wind

Wind speed changes have been observed across the global ocean over the last several decades that predominantly show increases in wind speed (Figure 2) [*Young et al.*, 2011]. Regionally, these increases can be strong, and only a few regions show decreasing wind trends. The magnitude of the flux is strongly

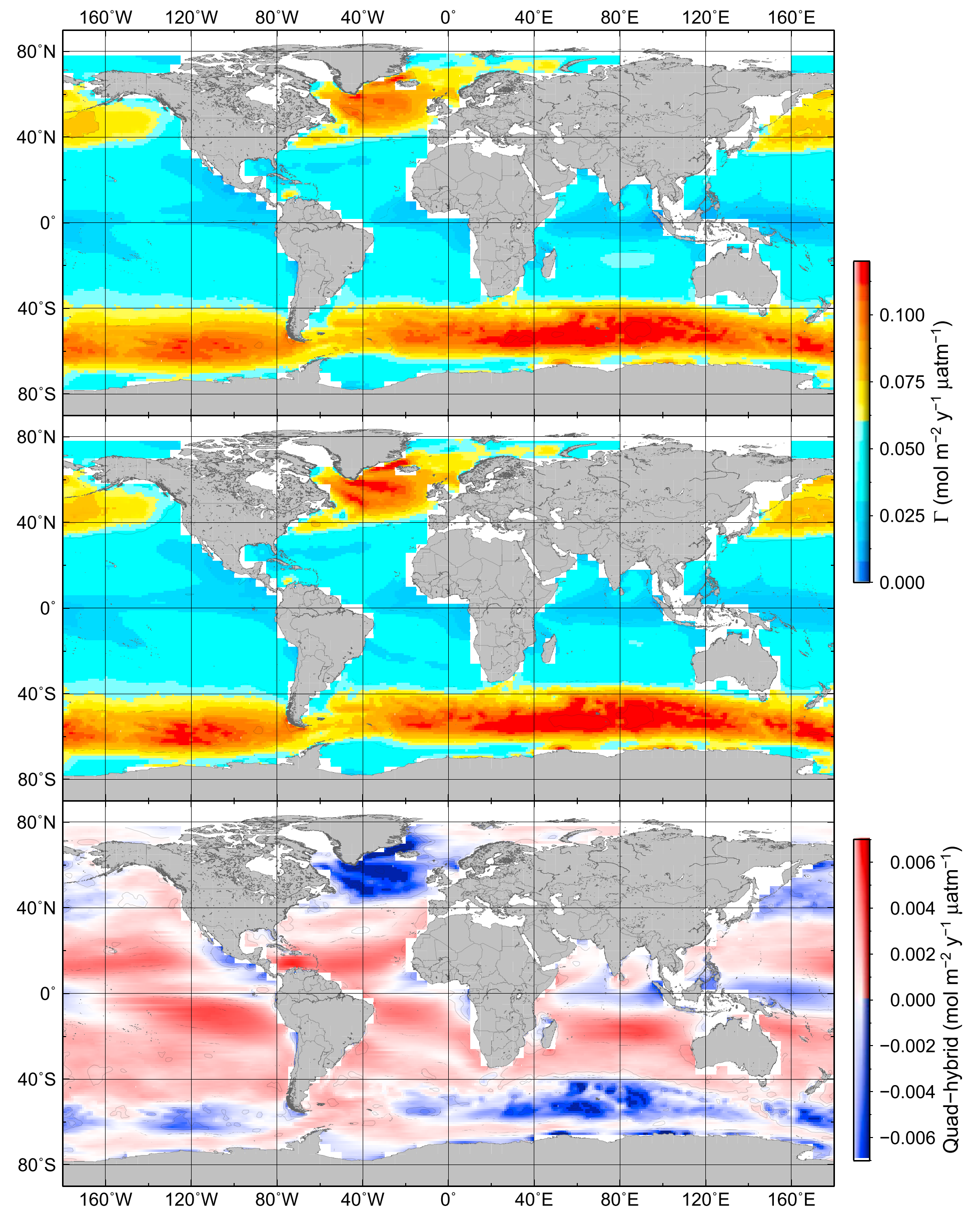

Figure 4. (top) Map of the mean gas exchange coefficient, Γ, for 2014 using a quadratic dependence. (middle) Map of the mean Γ for 2014 using the hybrid expression. (bottom) The difference between the quadratic dependence and the hybrid expression.

dependent on wind speed and its moments; therefore, the effect of the trends in wind on CO_2 fluxes will be a function of both the changes in variability of wind over time and its absolute magnitude. A numerical summary of the trends discussed is provided in the supporting information (Table S1).

Figure 3 (top) provides a global map of the mean wind speeds over the ocean for 2014. The annual average shows the prevailing high winds over the Southern Ocean with the maximum wind band centered at 50°S in the South Atlantic and Indian Oceans but farther south to 60°S in the Pacific Ocean with annual mean winds of ≈12 m s^{-1}. The lowest winds are in the equatorial band within 10° of the equator and in the subtropics. The high northern latitudes (40–60°N) show high winds, particularly in the North Atlantic. Figure 3 (bottom) shows the 27 year linear least squares fit of wind speed with time that represents the trend. Positive trends are observed for much of the ocean with the strongest trends in the tropical central Pacific (15°N–15°S) at ≈0.4 m s^{-1} decade^{-1}. There are local trends of similar magnitude in certain offshore regions, notably over

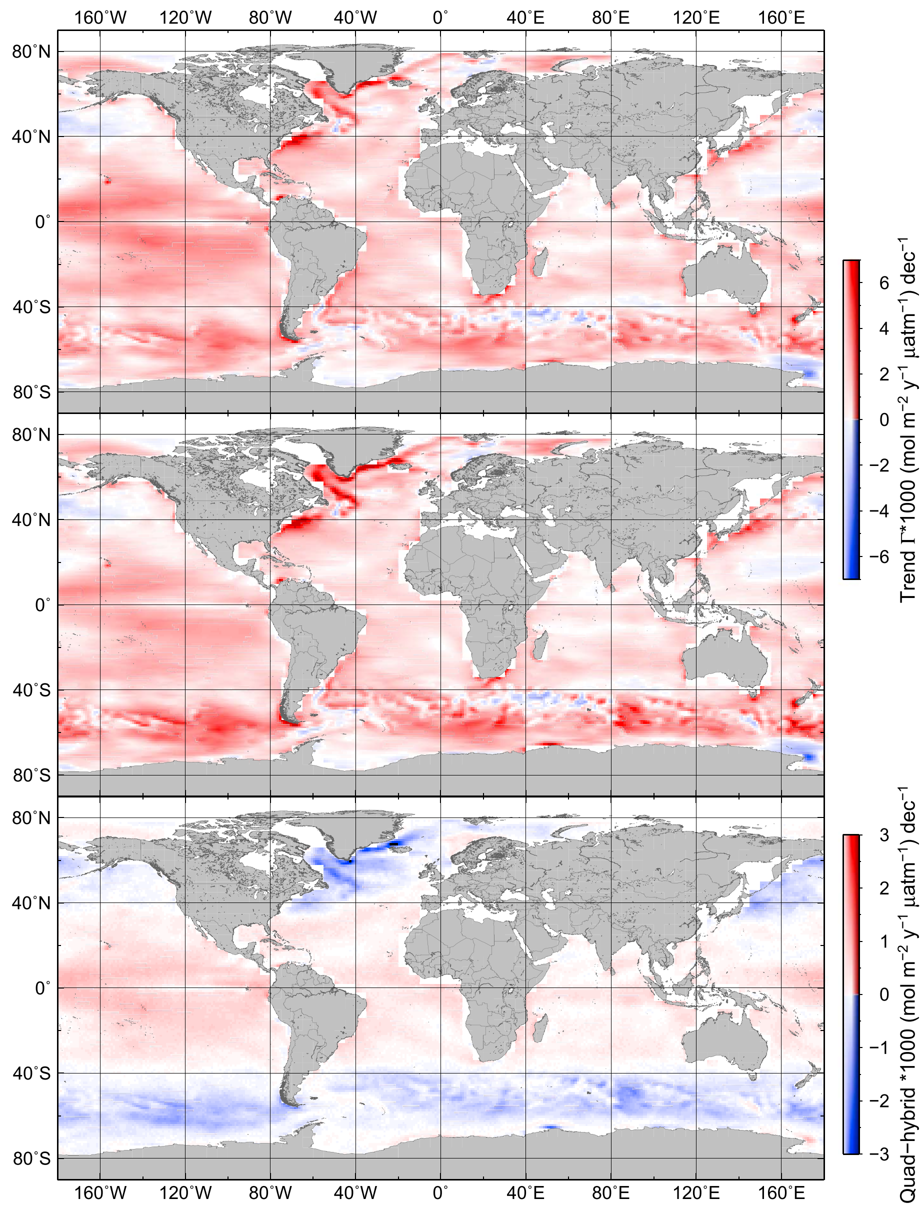

Figure 5. (top) Map of the trend in the gas exchange coefficient, Γ, for 1988–2014 using a quadratic dependence. (middle) Map of the trend in Γ using a hybrid expression. (bottom) The difference in trends in Γ between the quadratic dependence and hybrid expression. Units are (mol m^{-2} µatm^{-1}) decade^{-1}.

the Gulf Stream and off the coast of eastern and western South America. These increasing wind trends are associated with the sharp temperature gradients at the edge of boundary currents and are located on the warm side of fronts when the currents transport warm waters poleward into cold ocean regions [*Risien and Chelton*, 2008]. Weakly decreasing trends in winds (≈0.1 m s^{-1} decade^{-1}) are observed in the North Pacific between 40 and 50°N, western tropical Pacific centered at 20°N, and southern Indian Ocean centered at 40°S. There are also local decreases around the Antarctic continent. Variability in wind speed affects k [*Wanninkhof et al.*, 2002], but the trend in variability is small over the time period and does not affect the trend in k, as described in the supporting information (Figure S2).

3.2. Effect of the Trends in Wind on the Gas Transfer Coefficient

The gas transfer equations, equations (2) and (3), are for gases at the Schmidt number of 660, nominally CO_2 in seawater at 20°C. For determining in situ gas exchange rates, the product of the gas transfer velocity and

10.1002/2016GB005592

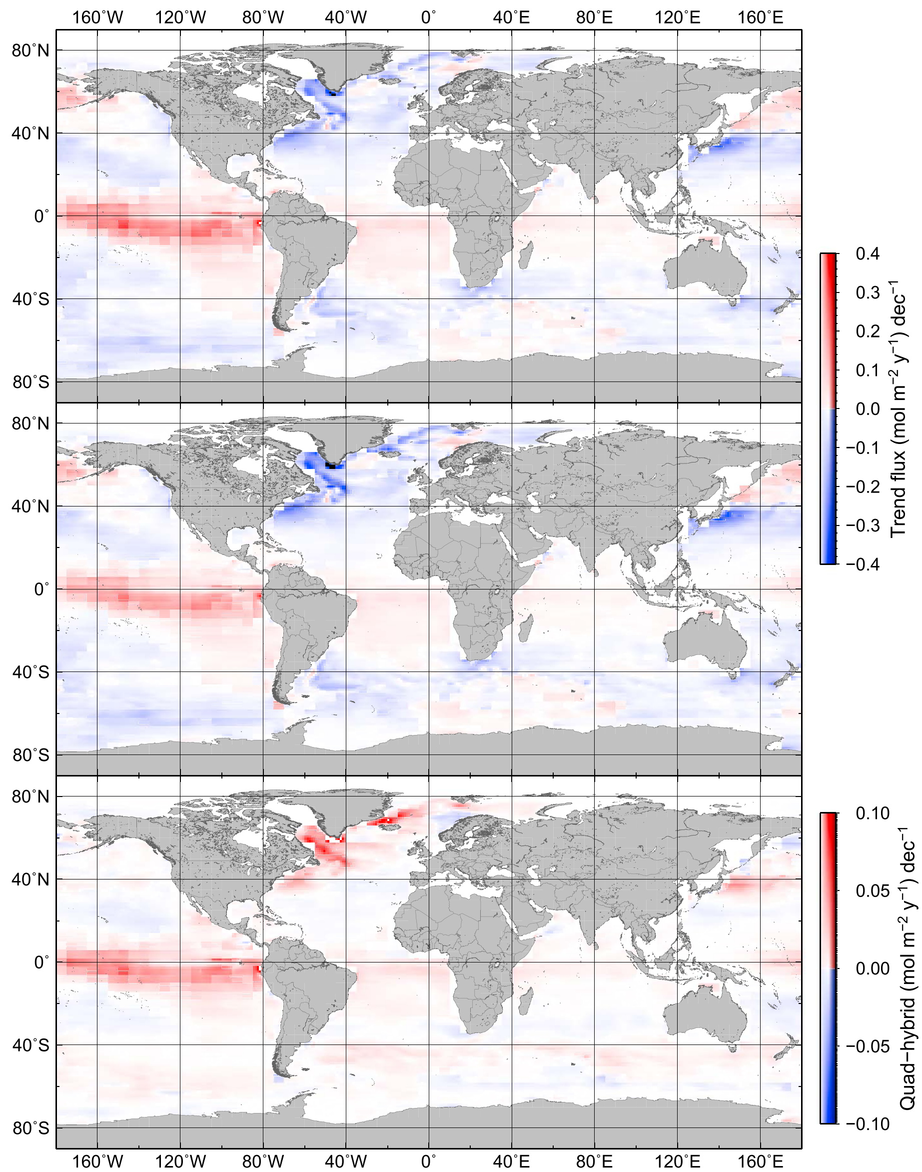

Figure 6. (top) Map of the trend in CO_2 fluxes for 1988–2014 using a quadratic dependence. (middle) Map of the trend in fluxes using a hybrid expression. (bottom) The difference in trends in fluxes between the quadratic dependence and hybrid expression.

solubility at in situ temperature, $(ks)_{\text{in situ}}$, Γ, is used. The Γ is dependent on the *Sc* and *s* of CO_2. As shown in Figure S1, the *Sc* of CO_2 decreases by about sevenfold, from −1 to 32°C, while $Sc^{-1/2}$ increases by a factor of 2.5. Solubility decreases by a factor of 3 such that Γ only decreases by about 10% over the oceanic temperature range.

The global pattern of Γ for 2014 is shown in Figure 4 with patterns closely following the global wind speed (Figure 3, top), indicating that the magnitude of Γ is largely controlled by *k*. The lowest values are observed in a narrow band along the equator, while the highest values straddle 50°N and 50°S. On a broad scale, the different parameterizations of gas transfer, equations (2) and (3), yield a very similar Γ, but their differences show a clear pattern (Figure 4, bottom). In subtropical regions with intermediate winds, the quadratic dependency yields a greater Γ, while the cubic dependency yields a higher transfer coefficient in regions of high winds centered at 50°N and 50°S and at low winds in the equatorial Indian and West Pacific Oceans. The latter is attributed to the nonzero intercept of the hybrid relationship (Figure 1).

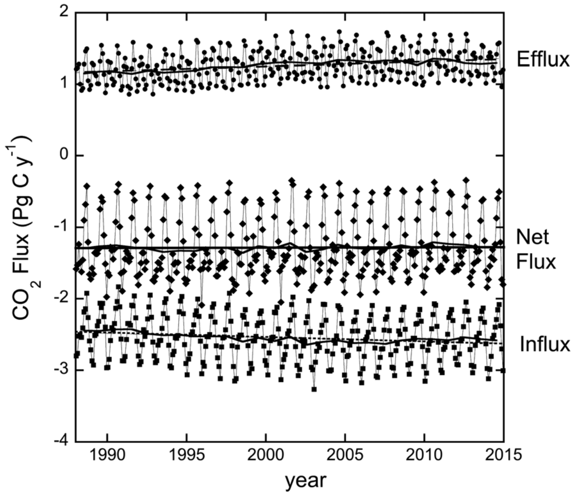

Figure 7. Monthly global CO_2 uptake (bottom, squares), net flux (center, diamonds), and efflux (top, circles) for 1988–2014 in Pg C y^{-1} using a fixed monthly ΔpCO_2 climatology. Annual fluxes are depicted by solid lines. The linear trends in efflux, net flux, and influx are shown as dashed, solid, and stippled lines, respectively.

The trends in Γ are shown in Figure 5. They follow the global wind speed trends but with a slight enhancement at higher latitudes, as the product of $((Sc/660)^{-1/2}$ s) shows a slight increase at lower temperatures (Figure S1). The trend of Γ is predominantly positive over the global ocean. Slight negative trends just north of 40°N in the Pacific Ocean and south of 40°S in the Indian Ocean are attributed to the poleward movement of the high wind speed belts as shown in Figure 3 (bottom), causing a decrease in Γ in these subpolar regions.

Comparing the quadratic and hybrid relationships of *k* with wind shows appreciably larger changes over the three decades for the hybrid dependency than the quadratic dependency in the regions with high winds at latitudes greater than 40°N and 40°S. For the remainder of the ocean, the quadratic dependency shows slightly greater trends in the tropics. There are large regions where the trends for the different parameterizations are largely the same (Figure 5, bottom). Changes due to ocean warming of ≈0.37°C over the time period cause a decrease in *s* of 1%, while $Sc^{-1/2}$ will increase by 0.9%, resulting in a negligible effect on Γ of CO_2.

3.3. Spatial Trends in Air-Sea CO_2 Fluxes

The direction of the flux is determined by the sign of the partial pressure difference of CO_2 between the water and air, ΔpCO_2 (equation (1)). Using the mean monthly pCO_2 climatology, there is a strong positive trend of increased outgassing in the equatorial Pacific and a negative trend in regions of net uptake in the North Atlantic and Southern Oceans, indicating increased uptake (Figure 6). Differences in the trends of the fluxes between the quadratic and hybrid gas transfer-wind speed relationships appear clearly in only two regions. The quadratic relationship shows more CO_2 outgassing in the central and eastern equatorial Pacific Ocean and less CO_2 uptake in the western boundary current regions of the Gulf Stream and Kuroshio currents. For most of the ocean, the different parameterizations have little effect on the trend of the fluxes.

3.4. Magnitude of the Global Trends in Air-Sea CO_2 Fluxes

The global impact of the trends in Γ on air-sea CO_2 fluxes depends on whether the changes in Γ occur in the source or sink regions. As indicated in Figure 6, the strongest trends in fluxes are observed in the source region of the equatorial Pacific Ocean and sink region of the Southern Ocean, suggesting that the increased sink strength is offset by the increased source strength. This is quantitatively borne out in Figure 7 that shows all the monthly 4° by 5° pixels of the Takahashi ΔpCO_2 climatology segregated into effluxes, $\Delta pCO_2 > 0$ µatm, and those with influxes, $\Delta pCO_2 < 0$ µatm [*Takahashi et al.*, 2014]. For the quadratic dependency, the trend in effluxes of 0.071 ± 0.009 (Pg C y^{-1}) decade^{-1} is opposite and greater than the trend of influxes of −0.05 ± 0.007 (Pg C y^{-1}) decade^{-1}, where the uncertainty is the root-mean-square error of the linear trend. The net result is a small decrease in the ocean sink of 0.015 ± 0.009 (Pg C y^{-1}) decade^{-1}. Figure 7 also shows that the monthly deviations in the effluxes and influxes are several orders of magnitude greater than the decadal trends, indicating that the month-to-month changes in wind have a much greater influence on global air-sea CO_2 fluxes than the long-term changes in wind.

Changes in the net efflux and net influx with the hybrid expression are 0.057 and −0.058 (Pg C y^{-1}) decade^{-1}, respectively, resulting in no significant net trend (0.0013 ± 0.009 (Pg C y^{-1}) decade^{-1}). Despite showing clear regional trends in Γ, the hybrid parameterization does not show a significant net effect of changing global

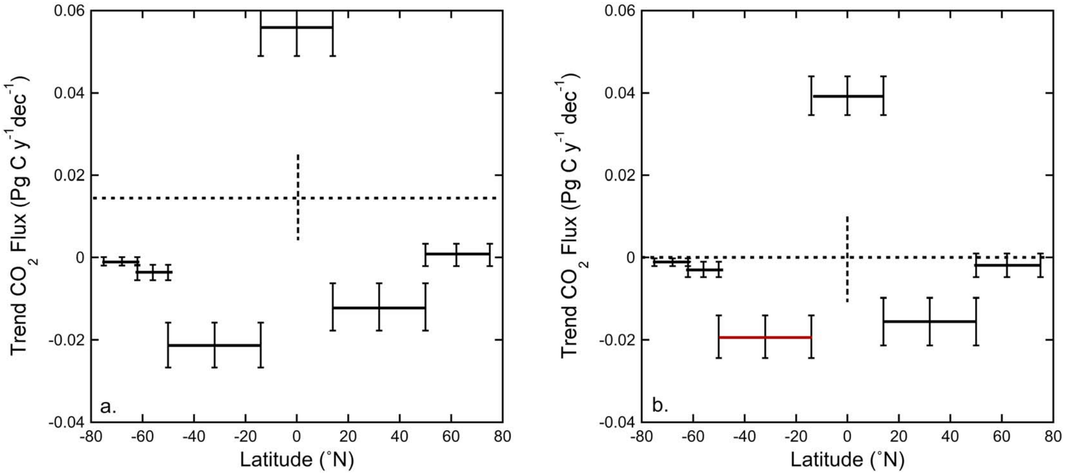

Figure 8. (left) Zonal distribution of the trends in CO_2 fluxes using a quadratic dependence. (right) Zonal distribution of the trends in CO_2 fluxes using a cubic dependence. The horizontal dashed lines are the global average trend, and vertical error bars are the standard error in the linear trends for each zone.

winds on air-sea CO_2 fluxes. Thus, depending on the parameterization, there is no global trend in global air-sea CO_2 fluxes as a result of increasing winds or a small decrease in CO_2 uptake by the ocean over the 27 year period.

Regional differences in the trends for Γ result in a smaller change in air-sea CO_2 fluxes over time than in a uniform change in wind over the ocean. If the increasing trend in global wind of 0.14 m s^{-1} $decade^{-1}$ was spatially uniform, the change in global uptake for the climatology of *Takahashi et al.* [2014] and the quadratic dependence would be −0.027 (Pg C y^{-1}) $decade^{-1}$. For the hybrid expression, the change in uptake would be −0.032 (Pg C y^{-1}) $decade^{-1}$. The change in flux discussed is in the opposite direction and at least twofold smaller at 0.015 (Pg C y^{-1}) $decade^{-1}$ and 0.001 (Pg C y^{-1}) $decade^{-1}$ for the quadratic and hybrid relationships, respectively. Thus, the effect of changing winds on fluxes depends critically on the patterns and locations of the wind speed changes and the pattern of ΔpCO_2.

The effect of changing Γ on air-sea CO_2 fluxes is much smaller than the changes in flux due to changes in ΔpCO_2 determined in other investigations that are summarized below. The ΔpCO_2 changes over time due to atmospheric increases and changes in water column processes, including those caused by wind forcing. Model-based estimates of increases in the air-sea CO_2 flux due to the release of anthropogenic CO_2 into the atmosphere is −0.15 (Pg C y^{-1}) $decade^{-1}$ [*Wanninkhof et al.*, 2013]. While there is currently insufficient ΔpCO_2 data to obtain annual global CO_2 fluxes from in situ surface water pCO_2 observations alone, several spatial and temporal observation-based interpolation techniques have been developed that provide estimates of global trends in ΔpCO_2 [*Park et al.*, 2010; *Landschützer et al.*, 2014; *Rödenbeck et al.*, 2015].

At the global scale, subdecadal variability dominates and impacts the magnitude of decadal changes. An average interannual variability of up to ±0.3 Pg C y^{-1} is observed for eight methods that extrapolate surface water pCO_2 [*Rödenbeck et al.*, 2015]. An observation-based mixed layer analysis using inverse constraints shows a decadal trend of +0.3 (Pg C y^{-1}) $decade^{-1}$ for 1990–2000, followed by an increase in the sink of −0.4 (Pg C y^{-1}) $decade^{-1}$ from 2000 to 2010 [*Rödenbeck et al.*, 2014]. The empirical observation-based approach of *Park et al.* [2010] that implicitly separates anthropogenic CO_2 forcing from changes induced by physical and biogeochemical forcing shows a trend of decreased uptake of ≈0.08 (Pg C y^{-1}) $decade^{-1}$ without anthropogenic CO_2 forcing. As detailed here, the global wind effect on Γ results in a change in flux of 0.001–0.015 (Pg C y^{-1}) $decade^{-1}$ and is appreciably smaller than the changes inferred from anthropogenic CO_2 forcing and changes in surface water CO_2 due to climate change and natural variability.

3.5. Regional Trends in Wind and Air-Sea CO_2 Fluxes

The effects of regional wind-induced trends in Γ on air-sea CO_2 fluxes largely counteract each other on a global scale. On regional scales, the trends in fluxes due to trends in wind on Γ are significant, particularly as the strongest trends in Γ occur over the largest source and sink regions. Figure 8 shows the zonal distribution of the trends in air-sea CO_2 fluxes using the oceanic regimes in *Takahashi et al.* [2009]. The negative trends in CO_2 fluxes in the subtropical and subpolar areas, as well as the polar regions of the Northern Hemisphere, are offset by the positive trend in the equatorial areas. The differences in the trends using either the quadratic (Figure 8, left) or hybrid (Figure 8, right) relationship are largely in the equatorial regions. The lower positive trend in this area using the hybrid expression causes the global trend to be close to zero over the period of investigation. For the quadratic expression, the net trend is slightly positive.

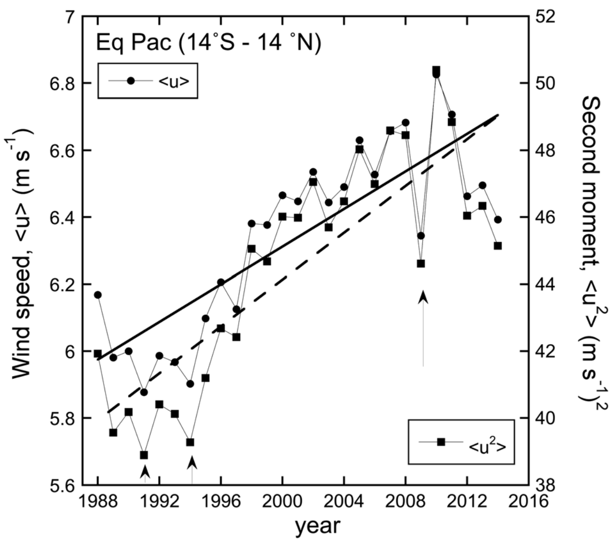

Figure 9. Annual average wind and the trend in wind (circles, solid line, left axis) and the second moment and trend in the second moment of the wind (squares, dashed line, right axis) in the equatorial Pacific (14°S–14°N). Arrows indicate the low winds during El Niño years.

The trends in the Southern Ocean, North Atlantic, and equatorial Pacific are further investigated using the quadratic and hybrid dependencies of wind speed on gas exchange. The equatorial Pacific, defined as the region from 14°N–14°S and 130°E–80°W, is the largest oceanic source of CO_2 due to upwelling. It is also the most variable on interannual timescales due to changes in upwelling associated with the ENSO [*Feely et al.*, 2006]. Superimposed on the large interannual variations in wind is a strong increasing trend in wind from 1988 to 2008. The trends of the annual mean wind, <*u*>, and the second moment of the wind, $<u^2>$, are shown in Figure 9.

During El Niño events the winds decrease, as observed in the record (Figure 9). The decadal trend in $<u^2>$ of 3.5 $(\text{m s}^{-1})^2$ decade^{-1} is heavily influenced by the prolonged El Niño conditions in the early 1990s, at the start of the CCMP-V2 wind product timeseries, and the strong La Niña with associated stronger winds in 2010–2011 near the end of the record. The trend from the peak of the El Niño period in 1993 to the strong La Niña conditions in 2010–2011 is 30% greater at 4.6 $(\text{m s}^{-1})^2$ decade^{-1} than the trend in the full record. The Γ increases by 7% decade^{-1} from 1988 to 2014, and the resulting CO_2 effluxes increase by 22% from ≈0.45 Pg C y^{-1} in the late 1980s to ≈0.55 Pg C y^{-1} in 2011 (Figure 10). Trends using the hybrid relationship are 30% less.

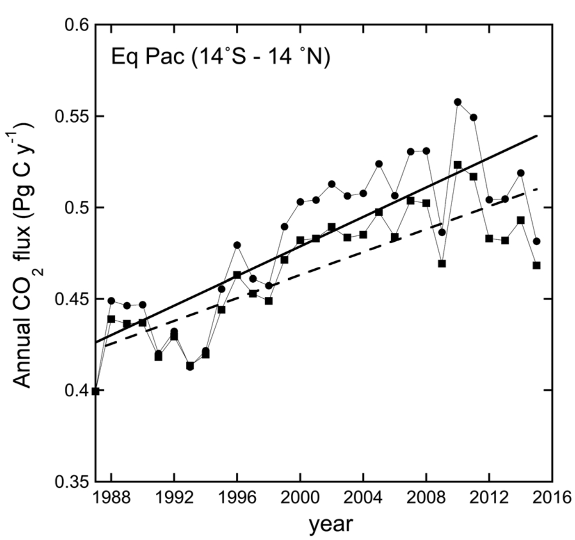

Figure 10. Annual average of CO_2 fluxes in the equatorial Pacific (14°S–14°N) for a quadratic dependence (circles and solid line) and hybrid expression (squares and dashed line).

The North Atlantic, defined as the region north of 50°N to the ice edge, is the strongest open ocean CO_2 sink on an areal basis. Increasing trends in the second moment of the winds are more than twofold less than in the equatorial Pacific with a $<u^2>$ of 1.4 $(\text{m s}^{-1})^2$ decade^{-1}. The annual winds are strongly dependent on the phase of the NAO, with negative NAO extremes showing annual winds

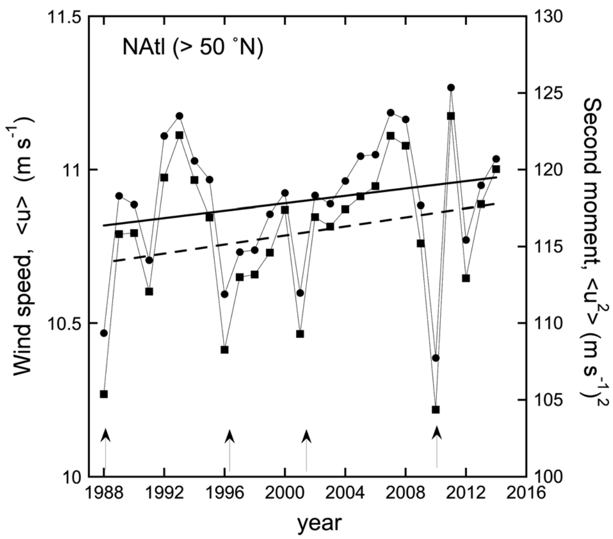

Figure 11. Annual average wind and linear trend (circles and solid line, left axis) and second moment of the wind and its linear trend (squares and dashed line, right axis) in the North Atlantic (>50°N). Arrows show the low annual winds during negative NAO anomalies.

≈0.5 m s^{-1} less than average years (Figure 11). The extremes in annual winds over the North Atlantic are more evenly distributed over the time period compared to the wind anomalies over the equatorial Pacific. Therefore, wind anomalies associated with the NAO have less of an effect on the decadal trends in Γ in the North Atlantic Ocean compared to the equatorial Pacific Ocean. The change in Γ is −1% $decade^{-1}$, and the uptake of CO_2 changes by −1% $decade^{-1}$ from approximately −0.255 to −0.262 Pg C y^{-1} $decade^{-1}$. Of note is that the negative trends in Γ and the flux when using the hybrid relationship are 46% greater at −1.5% and −1.6% $decade^{-1}$, respectively. This is because the hybrid relationship shows a stronger dependency on wind speed for the higher winds prevailing in the North Atlantic (Figure 1).

Winds in the high-latitude Southern Ocean (50–62°S) have increased appreciably since 1988 in response to the predominantly positive SAM during this period. The $<u^2>$ has increased by 1.4 (m $s^{-1})^2$ $decade^{-1}$ or about 2% $decade^{-1}$. These changes translate into a 2% increase per decade in Γ and a 3% increase per decade in CO_2 uptake, leading to a change in flux from an average of 0.078 Pg C y^{-1} to −0.085 Pg C y^{-1} from 1988 to 2014 for the quadratic relationship. The hybrid expression yields a ≈25% greater trend in Γ and corresponding CO_2 uptake. The changes in Γ using the hybrid expression are appreciably higher than using the quadratic expression because the winds are high in the region (Figure 12). Of note is that increasing winds will change ΔpCO_2 due to wind-induced upwelling. These changes in ΔpCO_2 lead to an opposite trend in CO_2 fluxes and a decrease in uptake over the last several decades [*Lovenduski et al.*, 2008] contrary to the effect of Γ on the fluxes. However, a reversal in the trend in CO_2 fluxes occurred in 2010 due to a more negative ΔpCO_2 [*Landschützer et al.*, 2015]. This again emphasizes that the trends in Γ have a secondary effect on the observed changes in air-sea CO_2 fluxes compared to changes in ΔpCO_2.

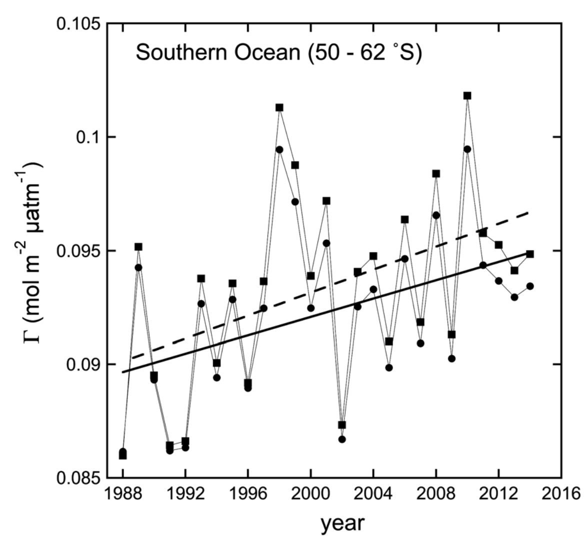

Figure 12. Annual average gas exchange coefficient, Γ, for the Southern Ocean between 50 and 62°S. The circles and solid line are the annual means and trend for Γ using the quadratic expression, while the squares and dashed line are the annual means and trend for Γ using the hybrid expression.

4. Conclusions

Global winds and, correspondingly, the gas exchange coefficient, Γ, have increased for much of the ocean since 1988. Strong regional trends in Γ are observed in the equatorial Pacific and Southern Ocean between

40 and 60°S. This has contributed to a change in air-sea CO_2 fluxes. However, the direct effect of wind on air-sea CO_2 fluxes through Γ is globally of secondary importance compared to changes in ΔpCO_2. Moreover, the changes in fluxes due to increases in Γ are appreciably smaller than inferred if there was a uniform increase in global winds over the ocean. Regional trends in gas fluxes caused by trends in Γ are greater in CO_2 source regions than the wind-induced trends of Γ in CO_2 sink regions. This results in an increase in the global ocean CO_2 source of 0.001–0.015 Pg C y^{-1} decade^{-1} rather than the 0.08 Pg C y^{-1} decade^{-1} increase in the global ocean CO_2 sink expected if increases in the wind were uniform over the ocean. The equatorial Pacific is the region most impacted by changing Γ over the observation period from 1988 to 2014, leading to an increase in outgassing due to the effect of winds on Γ of ≈0.1 Pg over two and a half decades. Predicting future changes in air-sea CO_2 fluxes will require accurate regional estimates of changes in wind and ΔpCO_2.

Acknowledgments

This work was sponsored by the Office of Oceanic and Atmospheric Research (OAR) of the National Oceanic and Atmospheric Administration (NOAA), U.S. Department of Commerce, including resources from the Ocean Observation and Monitoring Division of the Climate Program Office (fund reference 100007298) of NOAA. It was funded in part under the auspices of CIMAS under cooperative agreement NA10OAR4320143 with NOAA. We appreciate editing of the final version by Gail Derr of AOML. J. Shutler and an anonymous reviewer are acknowledged for their thoughtful input. Their comments and suggestions improved the final version. The cross-calibrated multiplatform (CCMP-V2) vector wind analyses are produced by Remote Sensing Systems with funding by NASA. Data are available at www.remss.com/measurements/ccmp and should be referenced as Wentz, F.J., J. Scott, R. Hoffman, M. Leander, R. Atlas, J. Ardizzone, 2015: Remote sensing systems cross-calibrated multiplatform (CCMP) 6-hourly ocean vector wind analysis product on 0.25° grid, version 2.0. Remote Sensing Systems, Santa Rosa, CA (Accessed 8 January 2016). The climatological pCO_{2w} data centered on 2005 were obtained from http://www.ldeo.columbia.edu/res/pi/CO2/carbondioxide/global_ph_data/obsfile.txt.

References

Atlas, R., R. N. Hoffman, J. Ardizzone, S. M. Leidner, J. C. Jusem, D. K. Smith, and D. Gombos (2011), A cross-calibrated multi-platform ocean surface wind velocity product for meteorological and oceanographic applications, *Bull. Am. Meteorol. Soc.*, *92*, 157–174, doi:10.1175/2010BAMS2946.1.

Bakker, D. C. E., et al. (2016), A multi-decade record of high-quality fCO_2 data in version 3 of the Surface Ocean CO_2 Atlas (SOCAT), *Earth Syst. Sci. Data*, *8*, 383–413, doi:10.5194/essd-8-383-2016.

Boutin, J., and J. Etcheto (1997), Long-term variability of the air-sea CO_2 exchange coefficient: Consequences for the CO_2 fluxes in the equatorial Pacific Ocean, *Global Biogeochem. Cycles*, *11*, 453–470, doi:10.1029/97GB01367.

Businger, J. A., and A. C. Delaney (1990), Chemical sensor resolution required for measuring surface fluxes by three common micrometeorological techniques, *J. Atmos. Chem.*, *19*, 399–410, doi:10.1007/BF00115782.

Butterworth, B. J., and S. D. Miller (2016), Automated underway eddy covariance system for air-sea momentum, heat, and CO_2 fluxes in the Southern Ocean, *J. Atmos. Oceanic Technol.*, *33*(4), 635–652, doi:10.1175/JTECH-D-15-0156.1.

Feely, R. A., T. Takahashi, R. Wanninkhof, M. J. McPhaden, C. E. Cosca, and S. C. Sutherland (2006), Decadal variability of the air-sea CO_2 fluxes in the equatorial Pacific Ocean, *J. Geophys. Res.*, *111*, CO8S90, doi:10.1029/2005JC003129.

Ho, D. T., R. Wanninkhof, P. Schlosser, D. S. Ullman, D. Hebert, and K. F. Sullivan (2011), Towards a universal relationship between wind speed and gas exchange: Gas transfer velocities measured with $^3He/SF_6$ during the Southern Ocean Gas Exchange Experiment, *J. Geophys. Res.*, *116*, C00F04, doi:10.1029/2010JC006854.

Kent, E. C., S. Fangohr, and D. I. Berry (2013), A comparative assessment of monthly mean wind speed products over the global ocean, *Int. J. Climatol.*, *33*(11), 2520–2541, doi:10.1002/joc.3606.

Landschützer, P., N. Gruber, D. C. E. Bakker, and U. Schuster (2014), Recent variability of the global ocean carbon sink, *Global Biogeochem. Cycles*, *28*, 927–949, doi:10.1002/2014GB004853.

Landschützer, P., et al. (2015), The reinvigoration of the Southern Ocean carbon sink, *Science*, *349*, 1221–1224, doi:10.1126/science.aab2620.

Le Quéré, C., T. Takahashi, E. T. Buitenhuis, C. Rödenbeck, and S. C. Sutherland (2010), Impact of climate change and variability on the global oceanic sink of CO_2, *Global Biogeochem. Cycles*, *24*, GB4007, doi:10.1029/2009GB003599.

Lovenduski, N. S., N. Gruber, and S. C. Doney (2008), Toward a mechanistic understanding of the decadal trends in the Southern Ocean carbon sink, *Global Biogeochem. Cycles*, *22*, GB3016, doi:10.1029/2007GB003139.

McNeil, C. L., and L. Merlivat (1996), The warm oceanic surface layer: Implications for CO_2 fluxes and surface gas measurements, *Geophys. Res. Lett.*, *23*, 3575–3578, doi:10.1029/96GL03426.

Monahan, A. H. (2006), The probability distribution of sea surface wind speeds. Part 1: Theory and SeaWinds observations, *J. Clim.*, *19*(4), 497–519, doi:10.1175/JCLI3640.1.

Olsen, A., R. Wanninkhof, J. A. Triñanes, and T. Johannessen (2005), The effect of wind speed products and wind speed-gas exchange relationships on interannual variability of the air-sea CO_2 gas transfer velocity, *Tellus*, *57B*, 95–106, doi:10.1111/j.1600-0889.2005.00134.x.

Park, G.-H., R. Wanninkhof, S. C. Doney, T. Takahashi, K. Lee, R. A. Feely, C. Sabine, J. Triñanes, and I. Lima (2010), Variability of global net sea-air CO_2 fluxes over the last three decades using empirical relationships, *Tellus*, *62B*, 352–368, doi:10.1111/j.1600-0889.2010.00498.x.

Peacock, S. (2004), Debate over the ocean bomb radiocarbon sink: Closing the gap, *Global Biogeochem. Cycles*, *18*, GB2022, doi:10.1029/2003GB002211.

Risien, C. M., and D. B. Chelton (2008), A global climatology of surface wind and wind stress fields from eight years of QuikSCAT scatterometer data, *J. Phys. Oceanogr.*, *38*(11), 2379–2413, doi:10.1175/2008JPO3881.1.

Rödenbeck, C., D. C. E. Bakker, N. Metzl, A. Olsen, C. Sabine, N. Cassar, F. Reum, R. F. Keeling, and M. Heimann (2014), Interannual sea-air CO_2 flux variability from an observation-driven ocean mixed-layer scheme, *Biogeosciences*, *11*, 4599–4613, doi:10.5194/bg-11-4599-2014.

Rödenbeck, C., et al. (2015), Data-based estimates of the ocean carbon sink variability—First results of the Surface Ocean pCO_2 Mapping intercomparison (SOCOM), *Biogeosciences*, *12*, 7251–7278, doi:10.5194/bg-12-7251-2015.

Sutton, A. J., R. A. Feely, C. L. Sabine, M. J. McPhaden, T. Takahashi, F. P. Chavez, G. E. Friederich, and J. T. Mathis (2014), Natural variability and anthropogenic change in equatorial Pacific surface ocean pCO_2 and pH, *Global Biogeochem. Cycles*, *28*, 131–145, doi:10.1002/2013GB004679.

Sweeney, C., E. Gloor, A. R. Jacobson, R. M. Key, G. McKinley, J. L. Sarmiento, and R. Wanninkhof (2007), Constraining global air-sea gas exchange for CO_2 with recent bomb ^{14}C measurements, *Global Biogeochem. Cycles*, *21*, GB2015, doi:10.1029/2006GB002784.

Takahashi, T., et al. (2009), Climatological mean and decadal change in surface ocean pCO_2, and net sea-air CO_2 flux over the global oceans, *Deep Sea Res., Part II*, *56*, 554–577, doi:10.1016/j.dsr2.2008.12.009.

Takahashi, T., S. C. Sutherland, D. W. Chipman, J. C. Goddard, C. Ho, T. Newberger, C. Sweeney, and D. W. Munro (2014), Climatological distributions of pH, pCO_2, total CO_2, alkalinity, and $CaCO_3$ saturation in the global surface ocean, and temporal changes at selected locations, *Mar. Chem.*, *164*, 95–125, doi:10.1016/j.marchem.2014.06.004.

Van Scoy, K. A., K. P. Morris, J. E. Robertson, and A. J. Watson (1995), Thermal skin effect and the air-sea flux of carbon dioxide: A seasonal high-resolution estimate, *Global Biogeochem. Cycles*, *9*, 253–262, doi:10.1029/94GB03356.

Wallcraft, A. J., A. B. Kara, C. N. Barron, E. J. Metzger, R. L. Pauley, and M. A. Bourassa (2009), Comparisons of monthly mean 10-m wind speeds from satellites and NWP products over the global ocean, *J. Geophys. Res.*, *114*, D16109, doi:10.1029/2008JD011696.

Wanninkhof, R. (2014), Relationship between wind speed and gas exchange over the ocean revisited, *Limnol. Oceanogr. Methods*, *12*, 351–362, doi:10.4319/lom.2014.12.351.

Wanninkhof, R., S. C. Doney, T. Takahashi, and W. R. McGillis (2002), The effect of using time-averaged winds on regional air-sea CO_2 fluxes, in *Gas Transfer at Water Surfaces*, *Geophys. Monogr. Ser*., vol. 127, edited by M. Donelan et al., pp. 351–357, AGU, Washington, D. C.

Wanninkhof, R., W. E. Asher, D. T. Ho, C. S. Sweeney, and W. R. McGillis (2009), Advances in quantifying air-sea gas exchange and environmental forcing, *Annu. Rev. Mar. Sci.*, *1*, 213–244, doi:10.1146/annurev.marine.010908.163742.

Wanninkhof, R., et al. (2013), Global ocean carbon uptake: Magnitude, variability and trends, *Biogeosciences*, *10*, 1983–2000, doi:10.5194/bg-10-1983-2013.

Weiss, R. F. (1974), Carbon dioxide in water and seawater: The solubility of a non-ideal gas, *Mar. Chem.*, *2*, 203–215, doi:10.1016/0304-4203(74)90015-2.

Young, I. R., S. Zieger, and A. V. Babanin (2011), Global trends in wind speed and wave height, *Science*, *332*, 451–455, doi:10.1126/science.1197219.